Monitoring deformation at The Geysers geothermal field, California using C-band and X-band Interferometric Synthetic Aperture Radar

D. W. Vasco,[1] Jonny Rutqvist,[1] Alessandro Ferretti,[2] Alessio Rucci,[2] Fernando Bellotti,[2] Patrick Dobson,[1] Curtis Oldenburg,[1] Julio Garcia,[3] Mark Walters,[3] and Craig Hartline[3]

D. W. Vasco, Jonny Rutqvist, Patrick Dobson, Curtis Oldenburg Earth Sciences Division/Building 74, Berkeley Laboratory, 1 Cyclotron Road, Berkeley, CA 94720. (e-mail:dwvasco@lbl.gov, JRutqvist@lbl.gov, pfdobson@lbl.gov, cmoldenburg@lbl.gov)

Alessandro Ferretti, Alessio Rucci and Fernando Bellotti, Tele-Rilevamento, Europa, Via Vittoria Colonna, 7-20149 Milano, Italy. (e-mail:alessandro.ferretti@treuropa.com, alessio.rucci@treuropa.com, fernando.bellotti@treuropa.com)

Julio Garcia, Mark Walters, and Craig Hartline, Calpine Corporation, 10350 Socrates Mine Road, Middletown, CA 95461. (e-mail: Julio.garcia@calpine.com, Mark.Walters@calpine.com, craig.hartline@calpine.com)

We resolve deformation at The Geysers geothermal field using two distinct sets of interferometric synthetic aperture radar (InSAR) data. The first set of observations utilize archived European Space Agency C-band synthetic aperture radar data from 1992 through 1999 to image the long-term and large-scale subsidence at The Geysers. The peak range velocity of approximately 50 mm/year agrees with previous estimates from leveling and global positioning system observations. Data from a second set of measurements, acquired by TerraSAR-X satellites, extend from May 2011 until April 2012 and overlap the C-band data spatially but not temporally. These X-band data, analyzed using a combined permanant and distributed scatterer algorithm, provide a higher density of scatterers (1122 per square kilometer) than do the C-band data (12 per square kilometer). The TerraSAR-X observations resolve 1 to 2 cm of deformation due to water injection into a Northwest Geysers enhanced geothermal system well, initiated on October 2011. The temporal variation of the deformation is compatible with estimates from coupled numerical modeling.

1. Introduction

The Geysers is the largest producing geothermal field in the world. The field is located in a complex tectonic environment and influenced by regional strain and Quaternary volcanism [*Oppenheimer*, 1986; *Prescott and Yu*, 1986; *Stanley et al.*, 1998; *Schmidt et al.*, 2003; *Funning et al.*, 2007]. In addition, there are local displacements due to injection and production at the geothermal field. The deformation in and around The Geysers has been documented using leveling data [*Lofgren*, 1981], trilateration observations [*Prescott and Yu*, 1986], and measurements made using the Global Positioning System (GPS) [*Mossop and Segall*, 1997, 1999]. Due to the magnitude of the deformation, roughly 5 cm/year [*Lofgren*, 1981; *Mossop and Segall*, 1997], and its widely distributed nature, it would seem that interferometric synthetic aperture radar (InSAR) could provide useful measurements of surface displacement [*Hanssen*, 2001]. Such observations have been used to image deformation associated with many geothermal fields [*Massonnet et al.*, 1997; *Carnec and Fabriol*, 1999; *Fialko and Simons*, 2000; *Vasco et al.*, 2002a; *Keiding et al.* 2010; *Eneva et al.*, 2012]. In this study we examine the utility of InSAR observations for monitoring deformation at The Geysers, using permanent and distributed scatterer techniques to derive estimates of the changes in the line-of-sight distance [the distance from a virtual radar antenna to an element on the ground] also known as range changes.

2. Interferometric Synthetic Aperture Radar Data

Two sets of InSAR data are considered in this study: (1) C-band measurements from the European Space Agency's ERS-1 and ERS-2 SAR satellites, and (2) X-band data from the TerraSAR-X satellite operated by the German Aerospace Center [*Eineder et*

al., 2009]. The C-band data, acquired between 1992 and 1999, were analyzed with the goal of estimating the regional deformation within and surrounding the geothermal field. During that time there were no large-scale water injections in the Northwest Geysers. The X-band data were gathered in 2011 and 2012 to obtain a localized estimate of the deformation induced by water injection in well Prati 32, in the Northwest Geysers. The spatial coverage of the two data sets overlap, providing an opportunity to compare the ability of each data set to image deformation at The Geysers.

2.1. ERS C-Band Observations

We applied a permanent scatterer algorithm to obtain estimates of the deformation within and around The Geysers. The permanent scatterer (PS) technique [*Ferretti et al.*, 2000; *Ferretti et al.*, 2001; *Ferretti et al.*, 2011] uses individual radar-bright and phase-stable objects on the Earth's surface (scatterers) to determine a time-series of the displacement of each scatterer projected onto the satellite's line-of-sight [*Colesanti et al.*, 2003]. The ERS descending track 113, frame 2817, encompasses the Geysers region. A total of 35 usable images, from June 13, 1992 until September 14, 1999, were processed to extract a collection of 31,680 permanent scatterers, shown in Figure 1. Due to vegetation and the lack of man-made structures, the coverage is non-uniform, with significant gaps in which there are no scatterers. The density of permanent scatterers is only about 12 per square kilometer, comparable to that of an earlier study of fault creep in an area just to the south of The Geysers [*Funning et al.*, 2007].

Subsidence is clearly visible in Figure 1 as an increase in range. The large-scale subsidence is attributed by many investigators to geothermal production at The Geysers.

Ongoing isostatic rebound of the 1.1 million year old felsite [*Stanley et al.*; 1998] into the overlying reservoir may also cause extension and subsidence in the region. The maximum range increase over the 7.25 year interval is 373.3 mm, leading to a range velocity of 51.5 mm/year, with an associated standard deviation of 0.5 to 1.5 mm/year. This value is in general agreement with previous subsidence estimates of 48 mm/year, obtained from leveling data between 1973 and 1977 [*Lofgren*, 1981], and an estimate of 47 mm/year calculated using GPS data from 1994 until 1996 [*Mossop and Segall*; 1997]. In order to compare the spatial coverage of the C-band measurements with the recently acquired TerraSAR X-band observations, we replot a subset of the data in Figure 2a above a radar amplitude image.

2.2. TerraSAR X-Band Observations

Lawrence Berkeley Laboratory and Tele-Rilevamento Europa (TRE) commissioned the TerraSAR-X satellite to monitor possible ground deformation associated with the water injection that is part of an enhanced geothermal system (EGS) project in the Northwest Geysers. The 29^o look-angle of the TerraSAR-X satellite is similar to the 23^o look-angle of the ERS satellites, resulting in range change estimates that are primarily sensitive to vertical displacement. Roughly one year of measurements, consisting of 29 images from May 2011 until April 2012, were used in the analysis. A relatively new processing technique, known as SqueeSAR [*Ferretti et al.*, 2011], uses a two-sample Kolmogorov-Smirnov test to partition image pixels into permanent (point-wise) scatterers, such as rock outcrops and man-made structures, and distributed scatterers such as rangeland, debris fields, scree, and bare earth. The permanent scatterers are processed in the manner

described in *Ferretti et al.* [2000; 2001] while the distributed scatterers are processed as statistically homogeneous subsets. The sub-division of scatterers into these two groups in indicated in Figure 2b. There is considerable overlap between regions containing point-wise or permanent scatterers (blue dots) and distributed scatterers (yellow areas). Plotting the scatterers upon digital images reveals that they are predominantly outcrops, regions of exposed soil and debris, portions of meadows between trees, and roads. The improvement in coverage provided by the X-band analysis can be seen by comparing the 1195 C-band estimates in the Northwest Geysers region (Figure 2a) with the much larger set of 112,231 X-band estimates for the same locale (Figure 2c).

3. Monitoring the Development of an Enhanced Geothermal System

In the Northwest Geysers EGS demonstration project, two abandoned exploration wells were re-opened, deepened, and recompleted in 2010 to form an injector/producer pair [*Garcia et al.*, 2012]. The surface-projected trajectories of the two wells are shown in detail in Figure 3a. On October 6, 2011 treated wastewater from the City of Santa Rosa was injected into the northernmost well, well Prati-32, at a rate of 1100 to 1200 gallons (4163 to 4542 liters) per minute. After 12 hours of injection [see Figure 3b], the rate was reduced to 400 gallons (1514 liters) per minute. This was maintained for 55 days, after which the injection rate was increased to 1000 gallons (3785 liters) per minute [*Garcia et al.*, 2012]. The production well Prati State-31 (PS-31) was chiefly used as an observation well during this time.

For six months preceding the injection, and during the injection period, InSAR data were gathered using the TerraSAR-X constellation of satellites. Concurrently, microseis-

micity was monitored by a high density seismic array and fluid pressures were recorded in two nearby observation wells, one of which is the well Prati State 31 (PS-31) [Figure 3b]. As part of a detailed analysis of the deformation in a region surrounding the EGS project, we considered all scatterers in the roughly one kilometer by one kilometer area shown in Figure 3a. The location of this detailed view is indicated by the small rectangle in each panel of Figure 2. To remove cyclical and long term trends common to all scatterers, an area-wide average displacement was subtracted from the range change for each time sample. Furthermore, long term trends were eliminated from each time series by fitting a linear trend from the pre-injection data and removing it from the entire series.

The detailed distribution of range change after 175 days of water injection is shown in Figure 3a. Range decreases, largely due to the uplift of the ground surface, are indicated by the unfilled squares. There are 558 estimates of range change in this figure and for each of these points we have 29 time samples, as indicated for two scatterers (AOYCB and AOXGB) in Figure 3b. We observe significant range decrease, of the order of 10 mm or more, primarily for points between the EGS injection and production wells. To the north and northwest of the injection well there are localized areas of range increase, denoted by the filled rectangles. Generally, the spatial wavelength of these localized range increases is of the order of a few hundred meters, suggesting shallow sources for the subsidence, perhaps due to landslides or local groundwater changes. It should be noted that there is another water injector, Prati 9, to the east of the EGS site that may induce uplift at the eastern edge of the region in Figure 3a.

4. Modeling the Deformation

We use the TOUGH-FLAC numerical simulator [*Rutqvist et al.*, 2002; *Rutqvist et al.*, 2010; *Rutqvist*, 2011] to model the coupled multiphase fluid flow, heat transfer, and deformation associated with the injection of cooler surface water into well P-32. The reservoir model consists of four layers: a graywacke-dominated caprock, a normal temperature (240^o C) reservoir, underlain by a high temperature (280-350^o C) zone of thermally-altered biotite hornfelsic metagrawacke and intercalated argillite, and finally a felsite layer [*Garcia et al.*, 2012]. Estimates of hydraulic properties were taken from a full field Geysers reservoir model, obtained by matching over forty years of injection and production data [*Rutqvist and Oldenburg*, 2008]. The permeability assigned to the normal temperature reservoir is $5 \times 10^{-14} m^2$ while in the high temperature reservoir the permeability is $2 \times 10^{-14} m^2$. The porosity of both reservoirs had to be reduced from the Calpine reference value of 1.0% to 0.4% in order to match the pressure increase due to the initial injection of the EGS project (Figure 3b). Initially, an average bulk modulus (K) of 5 GPa was used in the modeling, a value determined from an analysis of the subsidence of the entire geothermal field [*Mossop and Segall*, 1997]. A single linear thermal expansion coefficient of $0.00001^o/C$, obtained from measurements made on core samples at a temperature of 250^oC [*Mossop and Segall*, 1997], was also used in both reservoirs.

A total of 180 days of injection were modeled using the coupled TOUGH-FLAC simulator. The injection rate at P-32 and the fit to the observed pressure variation in the adjacent well PS-31 are shown in Figure 3b. Though we match the early pressure in PS-31 quite closely, the calculated pressure changes associated with the increase in injection rate

do deviate slightly from the observations. Such a deviation suggests a change in the state of the reservoir, perhaps due to pressure and/or temperature dependent changes in flow properties. For a comparison between observed and predicted range changes, we consider the deformation at two points: scatterer A0YCB [indicated by the circle in Figure 3a] and scatterer A0XGB [indicated by the star in Figure 3a], as shown in Figure 3b. In order to achieve a reasonable fit to the observed values at scatterer A0YCB, the average bulk modulus (K) of the host rock had to be increased by a factor of 3.2 to a value of 16 GPa. For scatterer A0XGB the bulk modulus was increased by almost twice that amount, a factor of 6.8 to a value of 34 GPa, in order to fit the observed range change.

5. Discussion

Interferometric synthetic aperture radar C-band data gathered over the entire Geysers geothermal field between 1992 and 1999 (Figure 1) indicate production-induced subsidence of roughly 5 cm/year, in agreement with estimates from previous studies [*Williamson* 1992; *Lofgren*, 1981; *Mossop and Segall*, 1997, 1999]. Newly available X-band data have improved spatial and temporal sampling, allowing for the direct monitoring of injection and production at individual wells. The improved coverage provided by the X-band data is likely due to two factors: an improved processing algorithm [*Ferretti et al.*, 2011] and better sampling properties associated with the TerraSAR-X satellites. The SqueeSAR algorithm jointly processes returns from stable point scatterers as well as from distributed scatterers. The TerraSAR-X satellites return every 11 days providing better the temporal coherence for distributed scatterers. Furthermore, the ground resolution of the X-band satellites is of the order of 3 m by 3 m, compared to the 20 m by 5 m resolution for the

C-band data. The improved resolution may allow for many additional stable returns from objects such as small to moderately sized outcrops.

The utility of X-band InSAR measurements at The Geysers is illustrated by an application to an enhanced geothermal system. Using a coupled numerical modeling code, and a reservoir model derived from historic subsidence data, we are able to match the temporal variation of the range change but not its magnitude. Specifically, we need a substantially higher bulk modulus in order to fit the magnitude of the range changes, as compared to the value estimated from matching the forty years of field-wide subsidence data. Distinct moduli for processes related to subsidence and uplift might be expected, considering the well established differences between virgin and elastic reservoir compressibility [*Teatini et al.*, 2011]. Factors related to the thermal contraction of the reservoir, due to the injection of relatively cool water, are included in the modeling and appear to be small in comparison to pressure induced deformation.

Heterogeneity is evident in the spatial variation of the range change plotted in Figure 3. For example, there is a significant difference in the observed range change at points A0YCB and A0XGB (Figure 3b) even though these scatterers are roughly the same distance from the injection well, and only about 150m apart. The heterogeneous pattern of deformation may reflect the influence of minor faults or fractures within the region. Indeed, the distribution of range changes and contemporaneous seismicity (Figure 3a) suggests preferential flow along a roughly north-south trending linear feature. The simultaneous spatial variation in geomechanical and flow properties across a narrow fault/fracture can result in rapid spatial variations in surface deformation [*Vasco et al.*, 2002b], particularly

if the feature extends to a shallower depth. Longer term monitoring, capturing both the uplift due to injection and the relaxation due to the cessation of pumping, should help in understanding the dominant flow due to the EGS.

6. Acknowledgments

This work was supported by the Assistant Secretary for Energy Efficiency and Renewable Energy, Geothermal Technologies Program of the U. S. Department of Energy under contracts DE-AC02-05CH11231 and DE-FC36-08G018201. Additional funding was provided by the Calpine Corporation.

References

Carnec, C., and H. Fabriol. Monitoring and modeling land subsidence at Cerro Prieto geothermal field, Baja California, Mexico, using SAR interferometry, *Geophysical Research Letters*, **26**, 1211-1214, 1999.

Colesanti, C., A. Ferretti, C. Prati, and F. Rocca. Monitoring landslides and tectonic motions with the permanent scatterers technique, *Engineering Geology*, **68**, 3-14, 2003.

Eineder, M., N. Adam, R. Bamler, N. Yague-Martinez, and H. Breit. Spaceborne spotlight SAR interferometry with TerraSAR-X, *Institute of Electrical and Electronics Engineers Transactions on Geoscience and Remote Sensing*, **47**, 1524-1535, 2009.

Eneva, M., D. Adams, G. Falorni, and J. Morgan. Surface deformation in Imperial Valley, CA, from satellite radar interferometry, *Geothermal Research Council Transactions*, **36**, 1339-1344, 2012.

Ferretti, A., C. Prati, and F. Rocca. Nonlinear subsidence rate estimation using permanent scatterers in differential SAR interferometry, *Institute of Electrical and Electronics Engineers Transactions on Geoscience and Remote Sensing*, **38**, 2202-2212, 2000.

Ferretti, A., C. Prati, and F. Rocca. Permanent scatterers in SAR interferometry, *Institute of Electrical and Electronics Engineers Transactions on Geoscience and Remote Sensing*, **39**, 8-20, 2001.

Ferretti, A., A. Fumagalli, F. Novali, C. Prati, F. Rocca, and A. Rucci. A new algorithm for processing interferometric data-stacks: SqueeSAR, *Institute of Electrical and Electronics Engineers Transactions on Geoscience and Remote Sensing*, **49**, 3460-3470, 2011.

Fialko, Y., and M. Simons, 2000. Deformation and seismicity in the Coso geothermal area, Inyo County, California: Observations and modeling using satellite radar interferometry, *Journal of Geophysical Research*, **105**, 21781-21793, 2000.

Funning, G. J., R. Burgmann, A. Ferretti, and A. Fumagalli. Creep on the Rodgers Creek fault, northern San Francisco Bay area from a 10 year PS-InSAR data set, *Geophysical Research Letters*, **34**, L19306, doi:10.1029/2007GL030836, 2007.

Garcia, J., M. Walters, J. Beall, C. Hartline, A. Pingol, S. Pistone, and M. Wright. Overview of the northwest Geysers EGS demonstration project, *37th Workshop on Geothermal Reservoir Engineering, Stanford University*, Stanford, 2012.

Hanssen, R., F. *Radar Interferometry*, Kluwer Academic Publishers, Dordrecht, 2001.

Keiding, M., T. Arnadottir, S. Jonsson, J. Decriem, and A. Hooper. Plate boundary deformation and man-made subsidence around geothermal fields on the Reykjanes Peninsula, Iceland, *Journal of Volcanology and Geothermal Research*, **194**, 139-149, 2010.

Lofgren, B. E. Monitoring crustal deformation in the Geyser-Clear Lake region. in *Research in The Geysers-Clear Lake geothermal area, Northern California*, U. S. Geological Survey Professional Paper, **1141**, United States Government Printing Office, 1981.

Massonnet, D., T. Holzer, and H. Vadon. Land subsidence caused by the East Mesa geothermal field, California, observed using SAR interferometry, *Geophysical Research Letters*, **24**, 901-904, 1997.

Mossop, A., and P. Segall. Subsidence at The Geysers geothermal field, N. California from a comparison of GPS and leveling surveys, *Geophysical Research Letters*, **24**, 1839-1842, 1997.

Mossop, A., and P. Segall. Volume strain within the Geysers geothermal field, *Journal of Geophysical Research*, **104**, 29113-29131, 1999.

Oppenheimer, D. H. Extensional tectonics at the Geysers geothermal area, California, *Journal of Geophysical Research*, **91**, 11463-11476, 1986.

Prescott, W. H., and S.-B. Yu. Geodetic measurements of horizontal deformation in the northern San Francisco Bay region, California, *Journal of Geophysical Research*, **91**, 7475-7484, 1986.

Rutqvist, J. Status of the TOUGH-FLAC simulator and recent applications related to coupled fluid flow and crustal deformation, *Computers and Geosciences*, **37**, 739-750, 2011.

Rutqvist, J., and C. M. Oldenburg. Analysis of injection-induced micro-earthquakes in a geothermal stream reservoir, Geysers Geothermal Field, California, *Proceedings of the 42th U. S. Rock Mechanics Symposium, San Francisco, California, USA*, **June 29-July 2, 2008**, 151, 2008.

Rutqvist, J., Y.-S., Wu, C.-F., Tsang, and G. Bodvarsson. A modeling approach for analysis of coupled multiphase fluid flow, heat transfer, and deformation in fractured porous rock, *International Journal of Rock Mechanics and Mining Sciences*, **39**, 429-442, 2002.

Rutqvist, J., C. M. Oldenburg, P. F. Dobson, J. Garcia, and M. Walters. Predicting the spatial extent of injection-induced zones of enhanced permeability at the Northwest Geysers EGS Demonstration Project, *Proceedings of the 44th U. S. Rock Mechanics Symposium, Salt Lake City, Utah, USA*, **June 27-June 30, 2010**, 502, 2010.

Schmidt, A. K., M. Grove, T. M. Harrison, O. Lovera, J. Hulen, and M. Walters. The Geysers-Cobb Mountain magma system, California (Part 2): Timescales of pluton emplacement and implications for its thermal history, *Geochemica et Cosmochimica Acta*, **67**, 3443-3458, 2003.

Stanley, W. D., H. M. Benz, M. A. Walters, A. Villasenor, and B. D. Rodriguez. Tectonic controls on magmatism in The Geysers-Clear Lake region: Evidence from new geophysical models, *Geological Society of America Bulletin*, **110**, 1193-1207, 1998.

Teatini, P., G. Gambolatia, M. Ferronatoa, A. Settari, and D. Walters. Land uplift due to subsurface fluid injection, *Journal of Geodynamics*, **51**, 1-16, 2011

Vasco, D. W., C. Wicks, K. Karasaki, and O. Marques. Geodetic imaging: reservoir monitoring using satellite interferometry, *Geophysical Journal International*, **149**, 555-571, 2002.

Vasco, D. W., K. Karasaki, and O. Nakagome. Monitoring production using surface deformation: the Hijiori test site and the Okuaizu geothermal field, Japan, *Geothermics*, **31**, 303-342, 2002.

Williamson, K. H. Development of a reservoir model for the Geysers Geothermal Field. *Monograph on the Geysers Geothermal Field*, Geothermal Resources Council Special Report **17**, 179-218, 1992.

7. Figure Captions

Figure 1. Range change determined from C-band measurements estimated using ERS-1 and ERS-2 data. Each colored pixel on this figure corresponds to a permanent scatterer and the color represents the range change in millimeters. Range decrease indicates movement towards the satellite (uplift) while range increases indicate movement away from the satellite, as due to subsidence. The outline of The Geysers geothermal field is indicated by a thick solid line. Regional faults are indicated by the thin solid lines. The rectangle denotes a region in which X-band interferometric synthetic aperture radar was gathered, shown in more detail in Figure 2. The insert shows the location of the Geysers-Clear Lake area within California.

Figure 2.

(a) C-band synthetic aperture radar (SAR) range velocity, extracted from a subset of the data in Figure 1. In order to facilitate a comparison with the X-band data, these measurements have been referenced to the same point as the TerraSAR-X data (-122.8186^o E, 38.8081^o N). We have converted the observations to range velocity in order to allow for a comparison of the changes over the two different time intervals: 1999-1992 and 2012-2011. The injection and production wells for the enhanced geothermal system experiment are denoted by the thicker solid lines. The rectangle indicates the area shown in Figure 3a.

(b) Color coded indication of scatterer type with distributed scatterers plotted as yellow regions and permanent or point-wise scatterers plotted as blue points. In regions of overlap the blue points are plotted over the yellow pixels.

(c) X-band estimated of range velocity derived from the TerraSAR-X data for the same region as in Figure 2a.

Figure 3.

(a) Detailed view of the range change in the region surrounding the injection well. Filled rectangles indicate a range increase and unfilled rectangles signify a range decrease. The size of each rectangle is proportional to the range change and the symbol in the lower left hand corner signifies 5 mm of range change. The circle indicates the location of scatterer A0YCB while the star denotes the location of scatterer A0XGB. The injection (P-32) and production (PS-31) wells are the labeled curves. The color map displays the density of earthquakes (number of earthquakes in a moving circular window of radius 100 m) for the time period between the start of injection (October 6, 2011) and the end of April 2012 (Figure 3a).

(b) (above) Flow rate data for injection well Prati-32 (P-32), indicated by the solid red line, along with the flow rate used in the reservoir simulation (dashed blue line). Pressure recorded in observation well Prati State 31 (PS-31) (solid green line) plotted against the pressure calculated during a numerical simulation, denoted by blue squares.

(below) Observed and calculated range changes associated with the two scatterers A0YCB and A0XGB. The individual points indicate observed values while the solid lines indicate range changes estimated from a coupled deformation and flow code. The values of the bulk moduli (K) required to match the range change data are indicated in the figure.

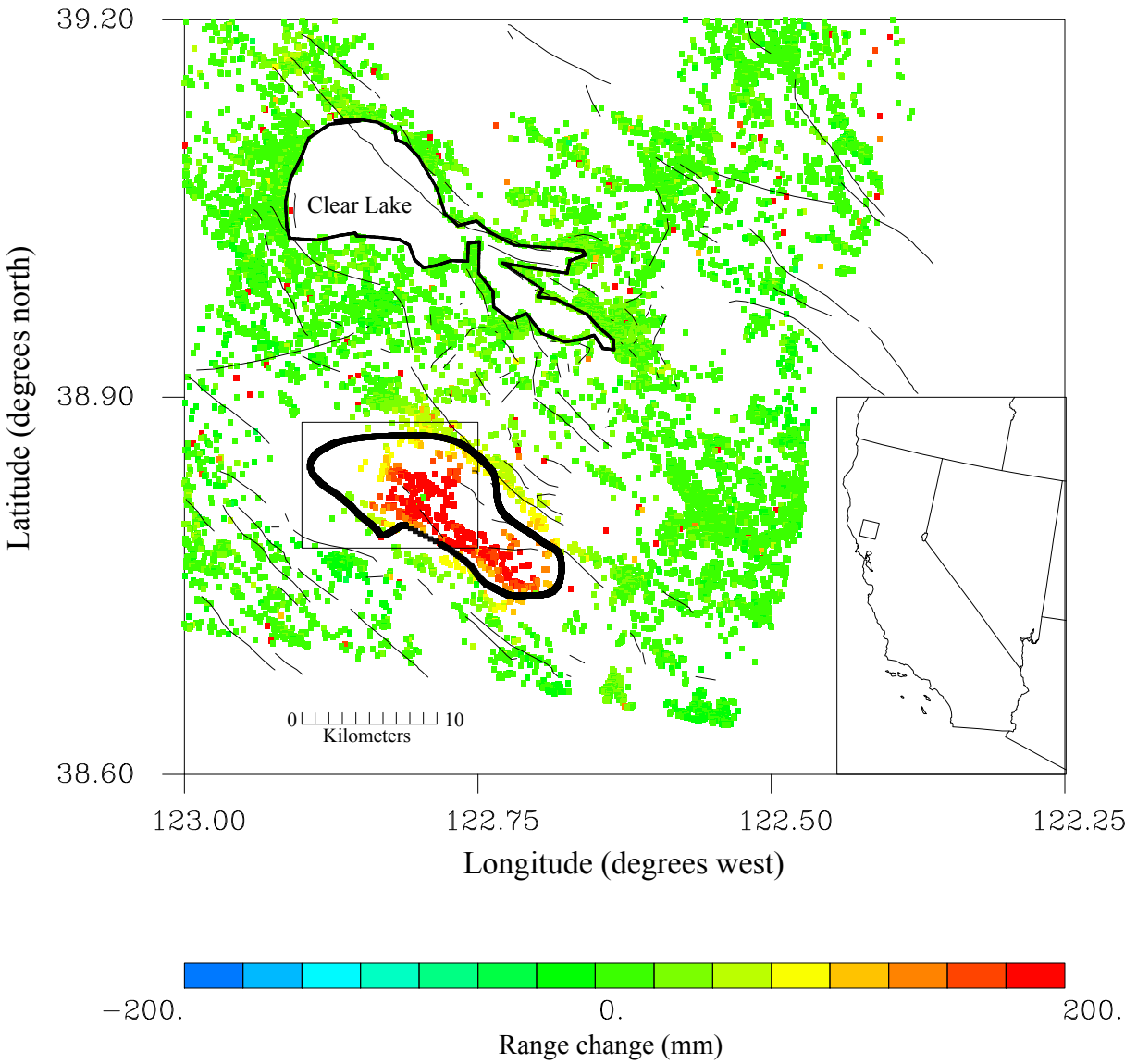
39.20
38.90
38.60
Latitude (degrees north)
Clear Lake
0
10
Kilometers
123.00
122.75
122.50
122.25
Longitude (degrees west)
−200.
0.
200.
Range change (mm)

Figure 1.

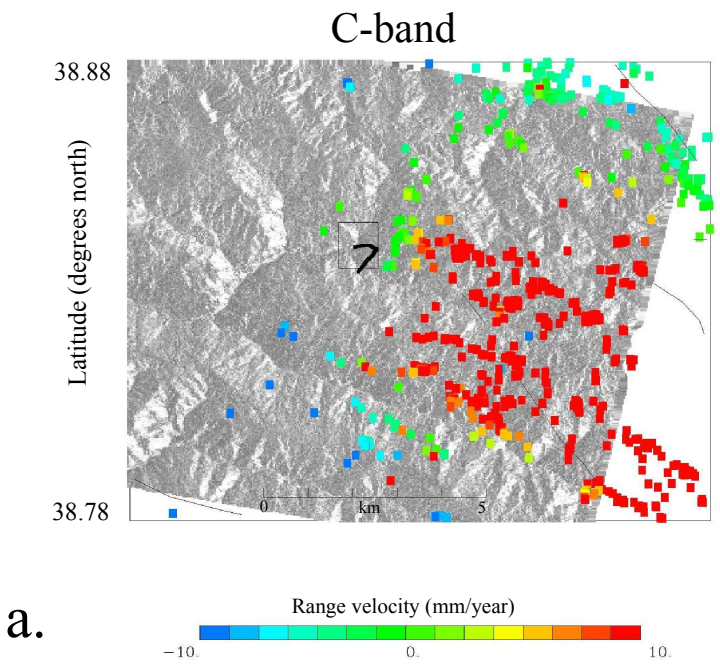
C-band
38.88
Latitude (degrees north)
38.78
0
km
5
Range velocity (mm/year)
−10.
0.
10.

a.

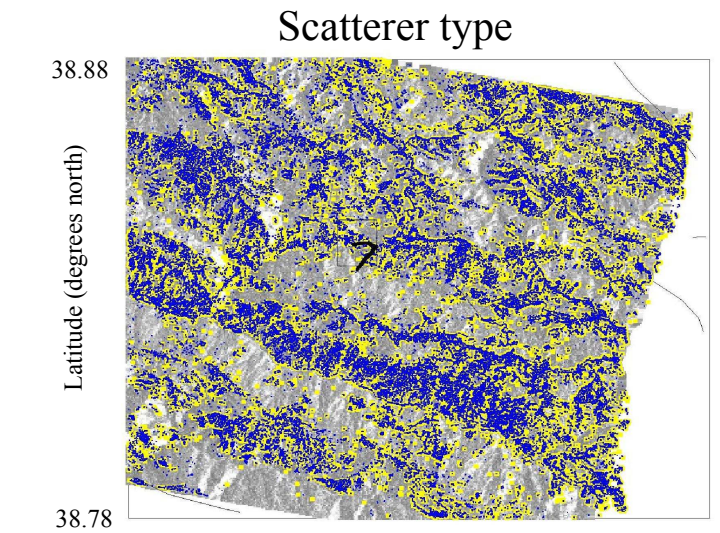
Scatterer type
38.88
Latitude (degrees north)
38.78

b.

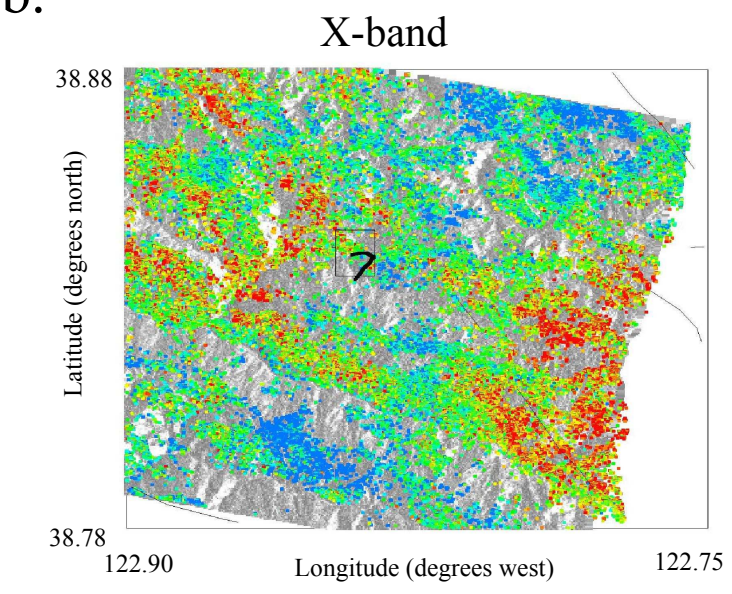
X-band
38.88
Latitude (degrees north)
38.78
122.90
Longitude (degrees west)
122.75
Range velocity (mm/year)
−10.
0.
10.

c.

Figure 2.

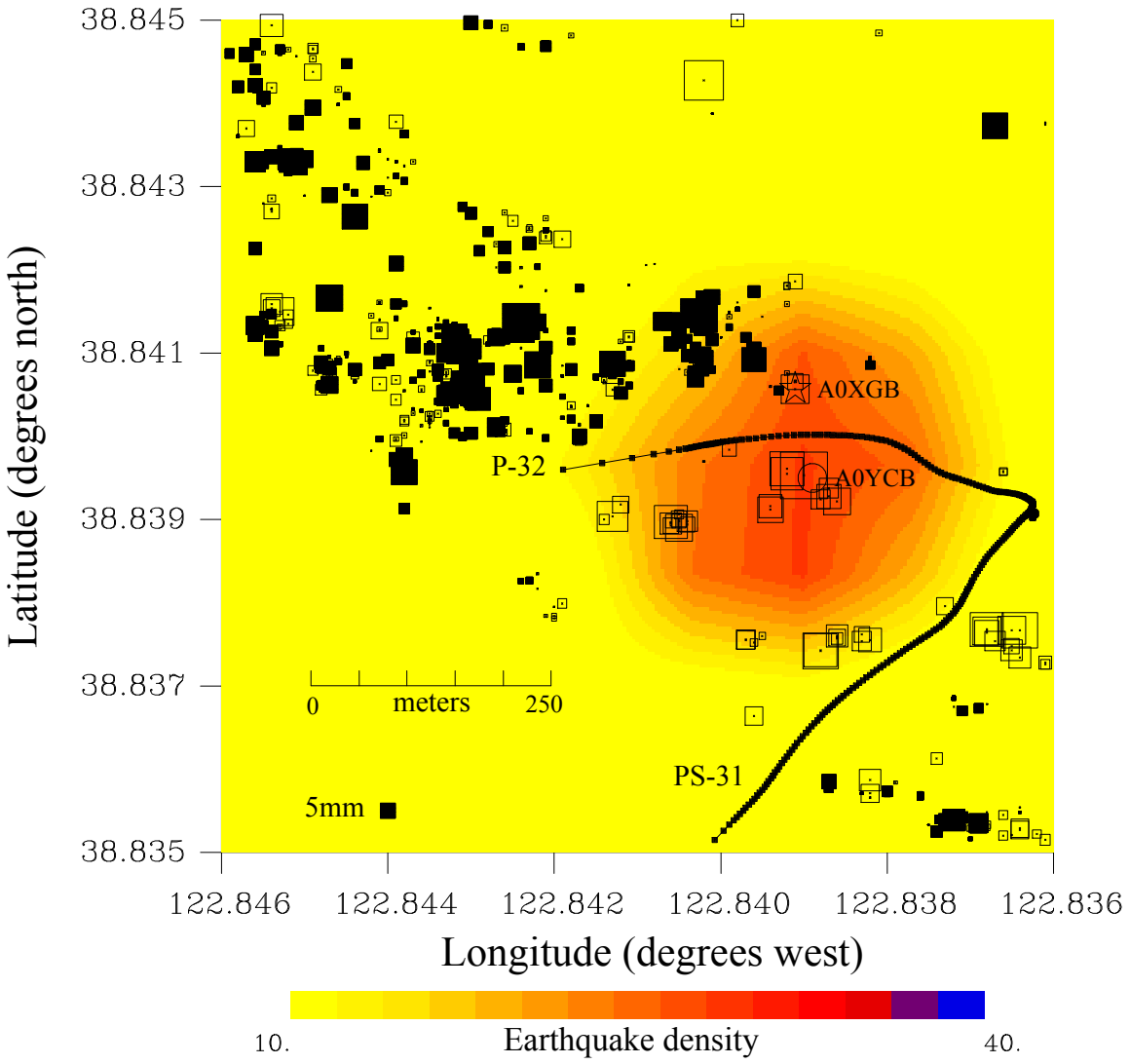
38.845
38.843
38.841
38.839
38.837
38.835
Latitude (degrees north)
A0XGB
P-32
A0YCB
0
meters
250
PS-31
5mm
122.846
122.844
122.842
122.840
122.838
122.836
Longitude (degrees west)
10.
Earthquake density
40.

Figure 3a.

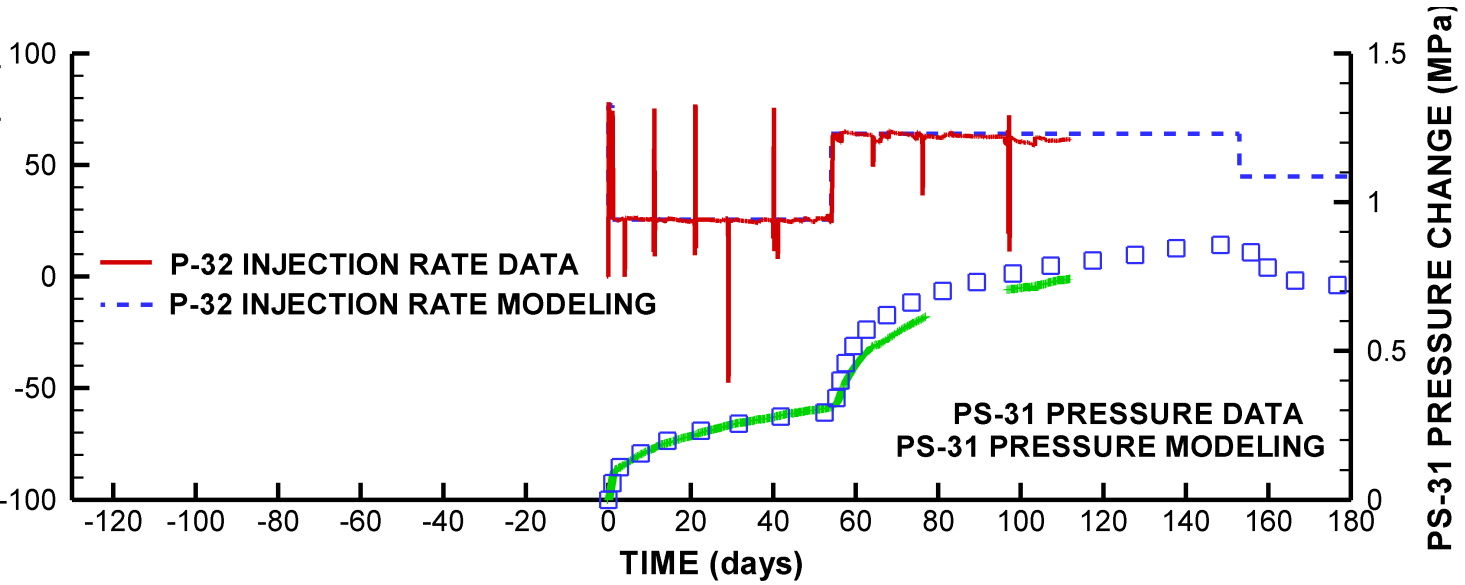
P-32 INJECTION RATE DATA
P-32 INJECTION RATE MODELING
PS-31 PRESSURE DATA
PS-31 PRESSURE MODELING
TIME (days)
PS-31 PRESSURE CHANGE (MPa)
100
50
0
-50
-100
1.5
1
0.5
0
-120 -100 -80 -60 -40 -20 0 20 40 60 80 100 120 140 160 180

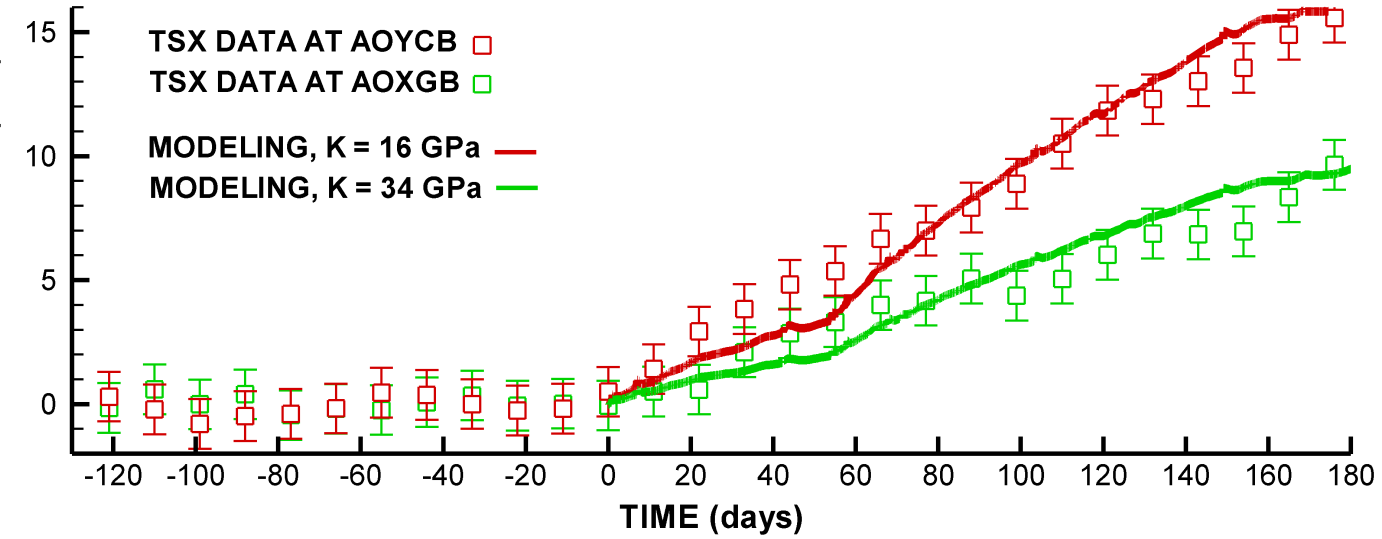
TSX DATA AT AOYCB
TSX DATA AT AOXGB
MODELING, K = 16 GPa
MODELING, K = 34 GPa
TIME (days)
15
10
5
0
-120 -100 -80 -60 -40 -20 0 20 40 60 80 100 120 140 160 180

Figure 3b.